Microchimica Acta (2018) 185: 327
https://doi.org/10.1007/s00604-018-2865-8

ORIGINAL PAPER

A nanohybrid composed of Prussian Blue and graphitic C_3N_4 nanosheets as the signal-generating tag in an enzyme-free electrochemical immunoassay for the neutrophil gelatinase-associated lipocalin

Fengling Zhang[1] · Hongbin Zhong[1] · Ying Lin[1] · Miaoxuan Chen[1] · Qingshui Wang[2] · Yao Lin[2] · Jiyi Huang[3]

Received: 16 April 2018 / Accepted: 4 June 2018 / Published online: 12 June 2018

Abstract

An enzyme-free electrochemical immunoassay is described for the neutrophil gelatinase-associated lipocalin (NGAL; a biomarker of kidney disease). Prussian Blue (PB) nanoparticles with redox activity were deposited on graphitic C_3N_4 nanosheets (g-C_3N_4) by in-situ reduction. A screen printed electrode (SPCE) was modified with antibody against NGAL, and the PB-g-C_3N_4 nanohybrid was used as the signal-generating tag for the secondary antibody against NGAL. Upon addition of target NGAL and of secondary antibody, a sandwich is formed on the SPCE. At an applied potential of typically 0.13 V (vs. Ag/AgCl), a well-defined voltammetric peak is observed that results from the presence of PB on the secondary antibody. Under optimal conditions, the peak current increases linearly in the 0.01 to 10 ng·mL^{-1} NGAL concentration range, and the detection limit is 2.8 pg·mL^{-1}. An average precision of <12% was accomplished in the batch-to-batch mode. Other disease-related biomarkers do not interfere. The accuracy and inter-laboratory validation of this method were evaluated for target NGAL detection in spiked human serum by using a commercial ELISA. The results obtained by the two methods are in good accordance.

Keywords Kidney biomarker · Transmission electron microscopy · Scanning electron microscopy · Method accuracy · Human serum specimens

Introduction

Neutrophil gelatinase-associated lipocalin (NGAL, a biomarker of kidney health, is a 24 kDa glycoprotein originally isolated from mouse kidney cells infected with a simian virus, SV-40. It shows promise in allowing a timely diagnosis of AKI since it is believed to be involved in renal development [1–3]. Although first discovered as a component of the late granules of neutrophils, NGAL is an indicator of kidney injury and released only when the kidney has come under duress from inflammation [4]. Urinary NGAL is produced in the renal tubule of the thick ascending limb of Henle and the collecting ducts [5]. Numerous studies have shown that the NGAL level in serum and urine is relative with the AKI severity. So, NGAL appears to fulfill many characteristics of an appropriate 'real-time' biomarker for AKI detection [6]. Early intervention significantly improves the prognosis.

Different schemes and strategies have been developed for the quantitative or qualitative determination of NGAL on the basis of various signal-generation principles, e.g., by up-

Fengling Zhang and Hongbin Zhong contributed equally to this work.

Electronic supplementary material The online version of this article (https://doi.org/10.1007/s00604-018-2865-8) contains supplementary material, which is available to authorized users.

✉ Yao Lin
yaolin@fjnu.edu.cn

✉ Jiyi Huang
hjy0602@163.com

[1] Xiang'an Branch, The First Affiliated Hospital of Xiamen University, Xiamen University, Xiamen 361003, China

[2] Provincial University Key Laboratory of Cellular Stress Response and Metabolic Regulation, College of Life Sciences, Fujian Normal University, Qishan Campus, Fuzhou 350117, China

[3] Medical College of Xiamen University, Xiang'an Branch, The First Affiliated Hospital of Xiamen University, Xiamen University, Xiamen 361003, China

converting phosphor technology-based lateral flow assay [7], tangential flow filtration and ion-exchange chromatography [8] and solid-phase proximity ligation assay [9]. Li et al. presented a label-free photoelectrochemical immunosensor for the NGAL detection by utilizing a biotinylated anti-NGAL nanobody-oriented TiO_2 electrode [10]. Kannan et al. developed a label-free electrochemical immunosensor for the NGAL detection by immobilizing rabbit polyclonal lipocalin-2 antibody on gold nanoparticles attached on PAMAM dendrimer-modified electrode [11]. Among these methods, electrochemical immunosensor have attracted great attention because of specific antigen-antibody reaction [12, 13]. For successful development of high-efficient electrochemical immunoassays, one of the most concerns for obtaining low limits of detection and quantification is to exploit advanced signal-generation tags [14]. Routine protocols usually involve in ligand-conjugated enzyme labels or nano labels. Undoubtedly, natural enzymes (e.g., horseradish peroxidase and alkaline phosphatase) are often employed as the signal-generation tags [15–17]. Unfavorably, the catalytic efficiency can be adequately implemented in the presence of electron mediators (e.g., ferricyanide, thionine or ferrocene derivatives) during electrochemical measurement [18, 19]. In this regard, the detection system may be contaminated, and the signal generation is unavoidable of interferences. Enzyme-substrate reaction is susceptible to incubation temperature and inhibitory substances [20]. Hence, an alternative immunosensing strategy that is based on an electrochemical principle and does not require an enzyme label would be advantageous. Prussian blue (PB; a typical hexacyanoferrate coordination compound with a low energy gap) exhibits unique electrocatalytic function since each neighboring iron in the chemical structure has two various valances, Fe(II) and Fe(III), for building the skeleton with the CN group [21, 22]. Interestingly, every adjacent twelve Fe-CN-Fe edges of the unit cell can form a large cavity to allow the entrance of alkali metal ions (e.g., Na^+ and K^+) for the increasing conductivity [23, 24]. To this end, our motivation of this study is to synthesize nanoheterostructures with Prussian blue nanoparticles (PB-NPs) on two-dimensional g-C_3N_4 nanosheets (i.e., a metal-free and nontoxic semiconductor with high thermal and chemical stability) thanks to atomic layer thickness, extraordinary physicochemical and biocompatible unique properties.

For facile ligand functionalization and biospecific interaction of electrochemical immunoassay, another important issue is to design a simple feasible sensing interface. Screen-printing technology seems to be one of the most suitable ways owing to its highly simplified reproducibility in serial production and inherent characteristics (e.g., miniaturization and inexpensive sensor production) [25]. The small-sized and integrated system with three electrodes in a single piece makes screen-printed electrodes ideal devices for fabrication of on-site electrochemical sensors [26]. Inspired by these advantages, we herein report on the proof-of-concept of simple and powerful immunosensing scheme for enzyme-free electrochemical detection of the NGAL (Scheme 1). PB-NP-decorated g-C_3N_4 nanosheets are first synthesized and functionalized with the anti-NGAL secondary antibody, whilst the immunosensor is fabricated on screen-printed graphite electrode (SPCE) by conjugating capture antibody with BSA in a saturated glutaraldehyde vapor. Accompanying the formation of the sandwich-type immunocomplex, the voltammetric signal derives from the labeled PB-NPs with the redox activity within the applied potentials. This work aims to develop an enzyme-free and on-site amplified electrochemical immunosensing protocol for the sensitive detection of low-abundance disease-related biomarker without the requirement of natural enzymes.

Materials and methods

Chemicals and reagents

Monoclonal mouse anti-lipocalin-2/NGAL antibody (mAb_1; Unconjugated; Reactivity: human; Clone: 5G5; Cat#:

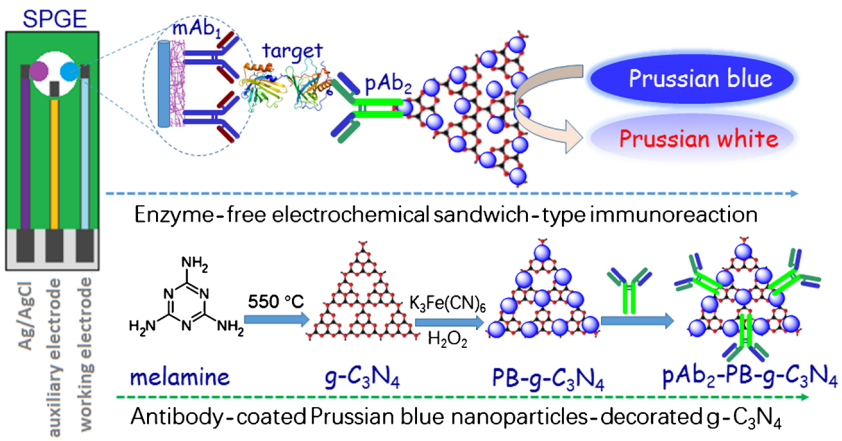

Scheme 1 Schematic illustration of the electrochemical immunoassay toward neutrophil gelatinase-associated lipocalin (NGAL) on monoclonal anti-NGAL antibody (mAb_1)-coated screen-printed graphite electrode (SPGE) by using polyclonal anti-NGAL antibody (pAb_2)-coated PB-NP-decorated g-C_3N_4 nanosheets (pAb_2/PB-g-C_3N_4)

ab23477) (note: Lipocalin-2 is also known as neutrophil gelatinase-associated lipocalin), polyclonal rabbit anti-lipocalin-2/NGAL antibody (pAb_2; Unconjugated; Reactivity: human; Cat#: ab41105) and human lipocaline-2 ELISA kit (Reactivity: human; Cat#: ab21554; Sensitivity: 14.8 pg mL^{-1}; Linear range: 46.9–3000 pg mL^{-1}) including the NGAL standards were purchased from Abcam (Cambridge, MA, USA www.abcam.cn). Glutaraldehyde solution (Grade I, 25 wt% in H_2O), bovine serum albumin (BSA; Vetec™, reagent grade, ≥98%) and melamine were obtained from Alfa (Shanghai, China www.alfa.com). These materials were used for preparation of screen-printing graphite electrode as follows: cyclohexanone (CA, No. C10, 218–0; Sigma-Aldrich), graphite power (No. 50870; Fluka), silver-based ink (GEM-Gwent, Pontypool, UK) and solid paraffin substrate (Alfa, Shanghai, China www.alfa.com). All other chemicals were of analytical grade and used as received. Ultrapure water obtained from a Millipore water purification system at 18.2 MΩ·cm (Milli-Q, Millipore www.merckmillipore.com) was used throughout this work. Phosphate buffered saline (PBS, 10 mM) with different pH values and containing 0.9% NaCl was used as the supporting electrolyte.

Synthesis of Prussian Blue nanoparticle-decorated g-C_3N_4 nanohybrids (PB-g-C_3N_4)

Prior to decoration with Prussian blue, water-dispersible g-C_3N_4 nanosheets were first prepared on the basis of typical wet-chemistry method (Please see the process in the Electronic Supporting Material) [27]. Then, PB-NP-decorated g-C_3N_4 nanohybrids (PB-g-C_3N_4) were synthesized via a hydrothermal method. Generally, 5.0 mL of aqueous mixture containing 2.5-mg g-C_3N_4 and 1.5-g $K_3Fe(CN)_6$ was kept into a vial under vigorous stirring for 30 min in an ice bath. Thereafter, 1.0 mL of 0.3 wt% H_2O_2 (pH 2.0) was added to the mixture, and continuously stirred for another 3 h. Following that, the reaction mixture was washed with pure water, centrifuged to remove the remaining reagents and dried at 60 °C. The prepared PB-g-C_3N_4 nanohybrids were stored in drying oven when not in use.

Preparation of mAb_1 antibody-coated screen-printed graphite electrode (mAb_1-SPGE)

First, screen-printed graphite electrode (SPGE) was prepared on a semi-automatic screen-printing machine (Please see the process in the Electronic Supporting Material). Then, the SPGE was modified with mAb_1 antibody by cross-linkage of the antibody with BSA in a saturated glutaraldehyde vapor. A homogenous mixture containing pAb_2 antibody (10 μL, 1.0 mg mL^{-1}) and BSA (10 μL, 10 wt%) was firstly deposited on the active area of the working electrodes via a drop method, then the resulting SPGE was placed in saturated glutaraldehyde vapor for 20 min, and then the resultant SPGE was dried at 4 °C for 12 h. Finally, the mAb_1-SPGE immunosensor was stored at 4 °C for use.

Immunoreaction protocol and voltammetric measurement

Scheme 1 represents schematic illustration of PB-g-C_3N_4-based electrochemical immunoassay for target NGAL on mAb_1-SPGE, using pAb_2/PB-g-C_3N_4 as the signal tag with a sandwiched reaction format. Prior to measurement, conjugation of PB-g-C_3N_4 nanohybrids with pAb_2 secondary antibody were prepared referring to the literature (Please see the process in the Electronic Supporting Material) [28]. The detection process toward NGAL was depicted as follows: (i) the mAb_1-SPGE was incubated with 30-μL PSA standard/sample for 35 min at room temperature; (ii) the resulting SPGE was submerged into the suspension containing pAb_2/PB-g-C_3N_4 (200 μL) and incubated for another 35 min under the same conditions; and (iii) square wave voltammetric (SWV) measurement from −50 mV to 350 mV (vs. Ag/AgCl) (Amplitude: 25 mV; Frequency: 15 Hz; Increase *E*: 4 mV) was collected on an AutoLab workstation (μAutIII.Fra2.v, Eco Chemie, Netherlands www.ecochemie.nl) and registered in a PBS (pH 6.8) as the signal of the immunosensor relative to NGAL level. After each step, the immunosensor was washed with pH 7.4 PBS. Impedimetric measurement was monitored at frequency 10^{-2} to 10^5 Hz at the formal potential of 220 mV, using alternating voltage of 10 mV. A Nyquist plot (Z_{re} vs. Z_{im}) was drown to analyze impedance results. All measurements were carried out at room temperature (25 ± 1.0 °C). The signals in all experiments referred to average responses of immunoreaction with corresponding standard deviations in triplicate, unless otherwise indicated.

Results and discussion

Choice of materials

To construct an electrochemical immunosensing platform for sensitive detection of low-abundance proteins, great attention has been focused on the signal amplification without the use of natural enzymes. Recent research has looked to develop innovative and powerful nanomaterials-based enzymatic mimics. In this case, the successful preparation of nanomaterials is very crucial in terms of reproducibility. Herein, mAb capture antibody is immobilized on the SPGE through a simple cross-linkage method with BSA in a saturated glutaraldehyde vapor, whilst pAb_2 secondary antibody is labeled to PB-NP-decorated g-C_3N_4 nanosheets by the

physical adsorption and entrapped technique. PB-NPs are utilized as the indicators with redox activity during the electrochemical measurement without the requirement of natural enzymes. Relative to the redox-active organic polymer nanoparticles alone, e.g., poly(Methylene Blue) or simple Prussian blue nanoparticles, introduction of g-C_3N_4 nanosheets is expected to enhance the amount of Prussian blue nanoparticles thanks to large surface coverage, thereby resulting in the amplification of the electrochemical signal. With a sandwich-type immunoassay format, the carried PB-g-C_3N_4 accompanying the secondary antibody increases with the increment of target NGAL. In this case, each of nanoparticle on the g-C_3N_4 nanosheets produces an electronic signal within the applied potentials. The change in the signal relies on the concentration of target NGAL in the sample with high sensitivity.

Characterization of PB-g-C_3N_4-based electrochemical immunoassay

To realize our design, preparation of mAb_1-SPGE and pAb_2/PB-g-C_3N_4 were very crucial for the successful development of the sandwich-type immunosensing system. Firstly, we used transmission electron microscopy (TEM, H-7605, Hitachi Instrumentation, Japan www.hitachi.co.jp) to characterize the synthesized g-C_3N_4 nanosheets (Fig. 1a) before and (Fig. 1b) after modification with Prussian blue. Figure 1a shows typical TEM image of g-C_3N_4 nanostructures, which exhibited a planar sheet-like morphology, suggested that the nanoscales were neither particles nor nanotubes. Such a sheet-like structure provides a large surface coverage for the immobilization of the PB-NPs. In contrast, the morphology of g-C_3N_4 nanosheets after reaction with $K_3Fe(CN)_6$ and H_2O_2 was obviously different from g-C_3N_4 alone (Fig. 1b vs. Fig. 1a). Numerous nanoparticles were coated on the surface of g-C_3N_4 nanosheets. Vaguely we seemed to observe that the lattice and shape of PB-NPs, as seen from high-solution transmission electron microscopy (HRTEM) (Fig. 1b, left inset). Since BSA protein was used for the synthesis of pAb_2/PB-g-C_3N_4, bioconjugation of pAb_2 antibody with PB-g-C_3N_4 nanosheets was very difficultly verified by using UV-vis adsorption spectroscopy and Fourier transform infrared spectroscopy. In this regard, we also used dynamic light scattering (DLS, Zetasizer Nano S90, Malvern, UK www.malvern.com) to characterize PB-g-C_3N_4 before and after modification with pAb_2 secondary antibody (Fig. 1b, top inset). Obviously, the average size of PB-g-C_3N_4 nanohybrids increased from 11.3 ± 1.2 nm to 20.6 ± 1.5 nm after coating with the antibody. These results revealed the successful preparation of PB-g-C_3N_4 for the labeling of pAb_2 secondary antibody.

The fabrication process of the mAb_1-SPGE immunosensor was characterized by using scanning electron microscopy (SEM; Hitachi SU8020, Japan www.hitachi.co.jp). Figure 1c gives typical TEM image of the newly screen-printed graphite electrode by using the cutting technique with the coated working electrode. The surface was very rough, which was not comparative with commercial glassy carbon electrode.

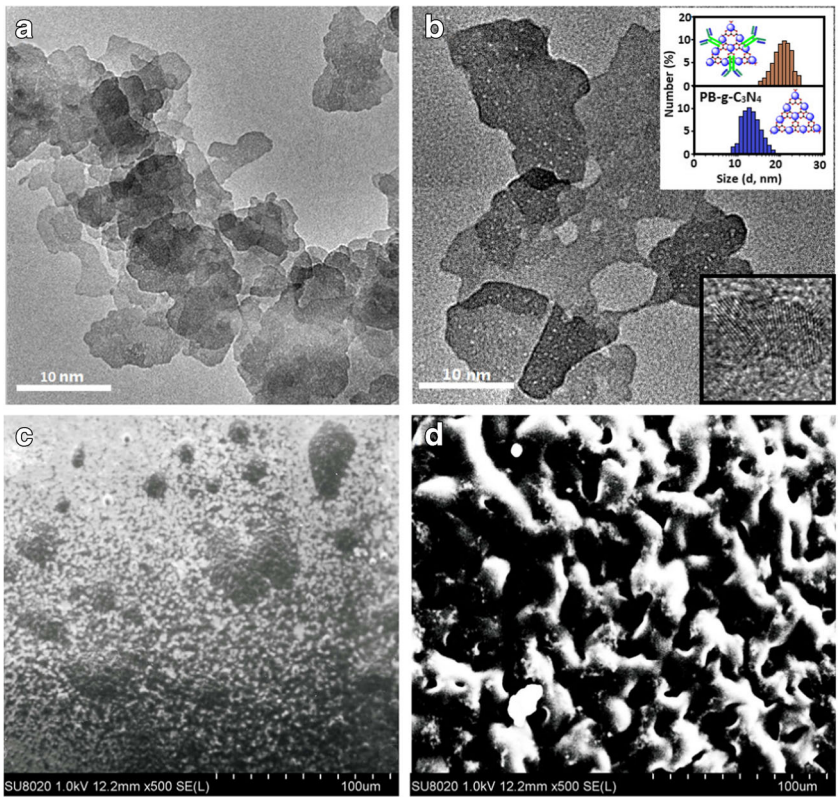

Fig. 1 Typical TEM images of **a** g-C_3N_4 nanosheets and **b** PB-g-C_3N_4 nanohybrids [insets: (top) DLS data of PB-g-C_3N_4 and pAb_2/PB-g-C_3N_4; (bottom) HRTEM image of PB-g-C_3N_4 nanohybrids]; TEM images of **c** the newly SPGE and **d** pAb_2-SPGE

Actually, such a rough surface was favorable for the immobilization of biomolecules in this work by the cross-linkage of the antibody with BSA in a saturated glutaraldehyde vapor. As shown in Fig. 1d, some additional materials were attached to the screen-printed graphite electrode after using the vapor-deposition technique, which derived from the cross-linked pAb_2 antibody with BSA through the glutaraldehyde. Thus, the successful preparation of mAb_1-SPGE and pAb_2/PB-g-C_3N_4 provided a necessary prerequisite for the development of electrochemical immunoassay.

Evaluation of feasibility and control experiments

Logically, one question arises as to whether the mAb_1-SPGE and pAb_2/PB-g-C_3N_4 can be used for the detection of target NGAL by using electrochemical detection technique. To verify this issue, cyclic voltammetric characteristics of the mAb_1-SPGE were monitored in PBS (pH 6.8) at 50 mV s^{-1} within the applied potentials from −300 mV to 500 mV after reaction with target NGAL and pAb_2/PB-g-C_3N_4 in sequence (note: 0.1 ng·mL^{-1} NGAL used as an example in this case) (Fig. 2a). No cyclic voltammetric peaks of interest were obtained at both mAb_2-SPGE (curve '*a*') and mAb_1-SPGE/NGAL (curve '*b*'). Introduction of target NGAL on mAb_1-SPGE caused the decreasing background currents, indicating that NGAL as a kind of biomacromolecules inhibited the electron communication between the solution and the electrode. When the resulting SPGE reacted again with pAb_2/PB-g-C_3N_4, significantly, a pair of well-defined redox peaks were appeared at 82 mV and 143 mV (vs. Ag/AgCl), respectively (curve '*c*'), which originated from the coated nanoparticles on g-C_3N_4 nanosheets. To further investigate whether the redox peaks derived from the nonspecific adsorption of the mAb_1-SPGE toward pAb_2/PB-g-C_3N_4, the immunosensor was used for direct incubation with pAb_2/PB-g-C_3N_4 in the absence of target NGAL. As seen from curve '*d*', the cyclic voltammogram was almost the same as that of mAb_1-SPGE alone (curve '*a*'). The result indicated that pAb_2/PB-g-C_3N_4 is not non-specifically adsorbed to the mAb_1-SPGE, further suggested that introduction of pAb_2/PB-g-C_3N_4 on the mAb_1-SPGE stemmed from the specific antigen-antibody reaction.

In addition to voltammetric characterization, the immunoreaction at each step were monitored by using electrochemical impedance spectroscopy (EIS) in 10 mM $Fe(CN)_6^{4-/3-}$ + 0.1 M KCl with the range from 10^{-2} Hz to 10^5 Hz at an alternate voltage of 5 mV (Fig. 2b). A Randles equivalent circuit is fitted on the basis of the EIS data (Fig. 2b, inset). Typically, the equivalent circuit involves in four components including electrolyte resistance (R_s), the lipid bilayer capacitance (C_{dl}), charge transfer resistance (R_{et}) and Warburg element (Z_w). Among these components, the lipid bilayer capacitance and charge transfer resistance are dependent on the dielectric and insulating features at the electrode/electrolyte interface. Hence, the diameter of semicircular Nyquist diagram stands for the electron transfer resistance (R_{et}). Plots '*a*' gives the Nyquist diagram of the newly screen-printed graphite electrode, and the resistance was ~490 Ohm. After formation of mAb_1-SPGE, the resistance increased to ~812 Ohm (diagram '*b*'), implied that the coated mAb_1 capture antibody inhibited the electron transfer of $Fe(CN)_6^{4-/3-}$ from the solution to the SPGE surface. Further, the combination of target NGAL with capture antibody increased the resistance (diagram '*c*'), which was in accordance with that of cyclic voltammetric result (Fig. 2a, curve '*b*'). Although PB-NPs display certain electrochemical activity, reaction of pAb_2/PB-g-C_3N_4 with the analyte also caused the increase in the resistance (diagram '*d*' vs. diagram '*c*'). The reason might be attributed to the fact that the nanohybrids and the labeled pAb_2 antibody acted as the inert layer to inhibit the electron transfer. Based on the results of cyclic voltammetric and EIS measurement, we might make a conclusion that the mAb_1-SPGE and pAb_2/PB-g-C_3N_4 can be employed for the detection of target NGAL.

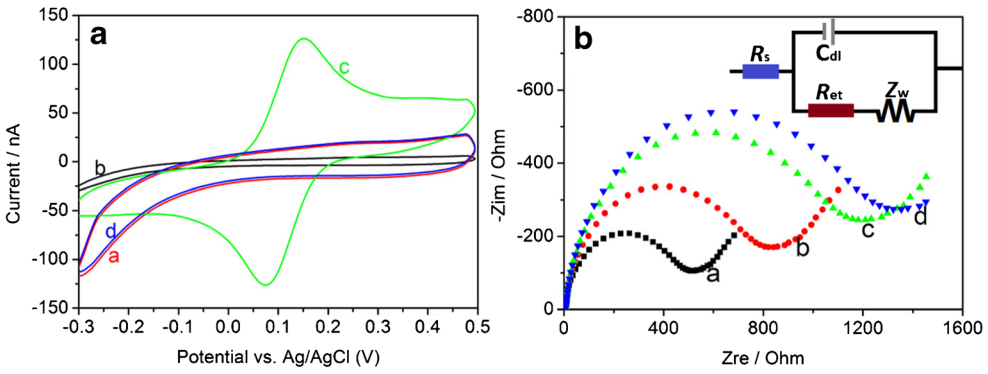

Fig. 2 **a** Cyclic voltammograms of (*a*) mAb_1-SPGE, (*b*) mAb_1-SPGE +0.1 ng·mL^{-1} NGAL, (*c*) sensor '*b*' + pAb_2/PB-g-C_3N_4 and (*d*) mAb_1-SPGE + pAb_2/PB-g-C_3N_4 at 50 mV·s^{-1} in PBS, pH 6.8; and **b** Nyquist diagrams for (*a*) SPGE, (*b*) mAb_1-SPGE, (*c*) mAb_1-SPGE +0.1 ng·mL^{-1} NGAL, (*d*) sensor '*c*' + pAb_2/PB-g-C_3N_4 in 10 mM $Fe(CN)_6^{4-/3-}$ + 0.1 M KCl with the range from 10^{-2} Hz to 10^5 Hz at an alternate voltage of 5 mV (inset: equivalent circuit)

Optimization of method

The following parameters were optimized: pH value, concentration of PB-NPs and incubation times. Respective data and Figures are given in the Electronic Supporting Material. The following experimental conditions were found to give best results: pH 6.8 PBS; 5.0 mL of an aqueous mixture containing 2.5-mg g-C_3N_4 and 1.5-g $K_3Fe(CN)_6$ for preparation of PB-g-C_3N_4, and 35 min for the antigen-antibody reaction.

Calibration plot

Under above-optimized conditions, the analytical properties of PB-g-C_3N_4-based electrochemical immunoassay were investigated toward target NGAL standards with different concentrations on the mAb_1-SPGE by using pAb_2/PB-g-C_3N_4 as the signal-generation tag with a competitive-type assay mode. SWV measurement was carried out in pH 6.8 PBS after the sandwiched immunocomplex. As shown in Fig. 3a, the SWV peak currents increased with the increasing NGAL concentration in the detection solution. Within the range of low-concentration or high-concentration NGAL samples, the voltammetric responses were not obvious, and exhibited a sigmoidal "*S*" relationship between the peak current and NGAL level. A good linear relationship between SWV peak current (nA) and the logarithm of NGAL concentration (ng mL^{-1}) was acquired within the dynamic range from 0.01 to 10 ng·mL^{-1} (Fig. 3b). The regression equation can be fit as y (nA) = 152.4 × log $C_{[NGAL]}$ + 309.3 (ng·mL^{-1}, R^2 = 0.9922, n = 7). The limit of detection (LOD) was estimated to 2.8 pg·mL^{-1}, which was based on the 3σ/m criterion (where σ is the standard deviation of the blank and m is the slope of calibration plot). The sensitivity was ~544.2 μA·μM^{-1}·cm^{-2}. Moreover, the LOD of our strategy was comparable with commercial human lipocalin-2/NGAL ELISA kits from various companies [e.g., 5.0 pg·mL^{-1} for Sigma (Cat#: RAB0332); 4.0 pg·mL^{-1} for Abcam (4.1–1000 pg·mL^{-1}; Cat#: ab113326); 14.8 pg·mL^{-1} for Abcam (46.9–3000 pg·mL^{-1}; Cat#: ab215541); 10 pg·mL^{-1} for Abcam (156–10,000 pg·mL^{-1}; Cat#: ab119600); 0.25 pg·mL^{-1} for Abcam (41.1–90,000 pg·mL^{-1}; Cat#: ab216816); 0.4 pg·mL^{-1} for Abcam (1.52–3333.33 pg mL^{-1}; Cat#: AB219024)], and other detection schemes (Table 1).

Precision, reproducibility, specificity and stability

The precision and reproducibility of PB-g-C_3N_4-based immunoassay were studied toward NGAL standards within six repeatedly assays by using the same-batch or different-batch mAb_1-SPGE and pAb_2/PB-g-C_3N_4. Three NGAL standards including 0.01, 0.1 and 10 ng·mL^{-1} were used in this case. The judgment was confirmed on the basis of relative standard deviation (RSD) during six analyses per sample. As indicated from experimental results, the RSDs was as follows: 9.2%, 4.3 and 5.6% (n = 6) for the intra-assays, and 10.7%, 9.8 and 11.2% (n = 6) for the inter-assays toward the aforementioned standards, respectively, thus suggested good reproducibility.

Next, the specificity of PB-g-C_3N_4-based electrochemical immunoassay was investigated toward target NGAL against other possible disease-related biomarkers in human serum, e.g., cancer antigen 15–3 (CA 15–3), alpha-fetoprotein (AFP), carcinoembryonic antigen (CEA), cancer antigen 19–9 (CA 19–9), cancer antigen 125 (CA 125) and prostate-specific antigen (PSA). These non-target analytes alone or co-existed with NGAL were determined by the electrochemical immunoassay. In this case, the ratio in the concentration between target NGAL and non-target analyte was 1: 100. As shown from Fig. 3c, the SWV peak currents toward non-target analytes were almost the same as that of background signal, and the strong current was obtained for target NGAL. Moreover, the coexistence of non-target analytes with NGAL did not significantly interfere the electrochemical

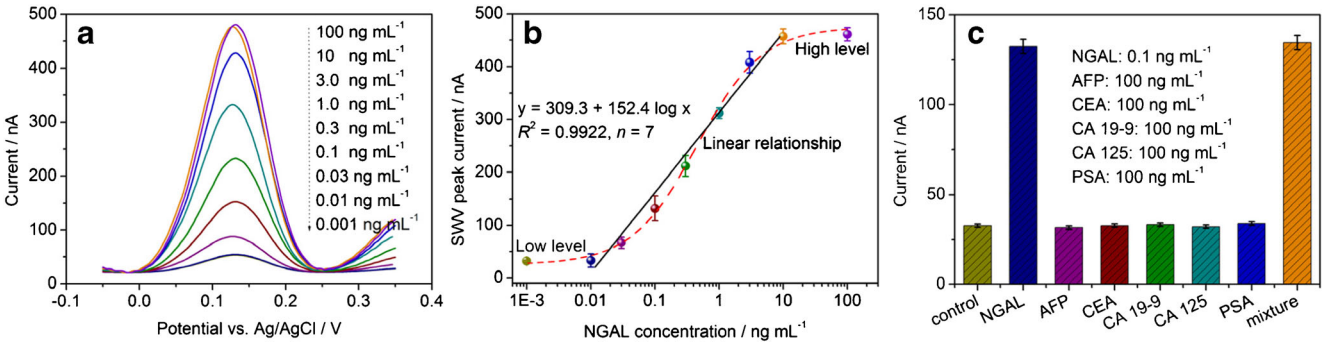

Fig. 3 **a** SWV response curves of mAb_1-SPGE-based immunosensor toward target NGAL with different levels from 0.001 to 100 ng·mL^{-1} by using pAb_2/PB-g-C_3N_4 as the signal-generation tag in PBS (pH 6.8); **b** the corresponding calibration plots; and **C** the specificity of PB-g-C_3N_4-based electrochemical immunoassay was investigated toward target NGAL against other possible disease-related biomarkers in human serum, e.g., cancer antigen 15–3 (CA 15–3), alpha-fetoprotein (AFP), carcinoembryonic antigen (CEA), cancer antigen 19–9 (CA 19–9), cancer antigen 125 (CA 125) and prostate-specific antigen (PSA) (note: The mixture contained the above- mentioned analytes) (n = 3)

Table 1 An overview on recently reported nanomaterial-based electrochemical methods for determination of lipocalin-2/NGAL

Materials used[a]	Method applied	Linear range	LOD	Ref.
Upconverting nanoparticles	Lateral flow assay	7.68–1000 ng·mL^{-1}	7.68 ng·mL^{-1}	[7]
Enzymatic DNA ligation	Solid-phase proximity ligation assay	–	6.4 pg·mL^{-1}	[9]
Nanobody	Photoelectrochemical immunosensor	0.001–500 ng·mL^{-1}	0.6 pg·mL^{-1}	[10]
AuNPs/PAMAM	Electrochemical immunosensor	50–250 ng·mL^{-1}	1.0 ng·mL^{-1}	[11]
PB-g-C_3N_4	Electrochemical immunosensor	0.01–10 ng·mL^{-1}	2.8 pg·mL^{-1}	This work

[a] AuNPs/PAMAM: gold nanoparticles attached on generation-1 poly(amidoamine) dendrimer

signal of the immunoassay. Hence, PB-g-C_3N_4-based immunoassay had good specificity.

Additionally, the lifetime of the mAb_1-SPGE by using pAb_2/PB-g-C_3N_4 was also monitored by keeping them in refrigerator at 4 °C when not in use. They were used for the detection of 10 ng·mL^{-1} NGAL (used as an example) every five days. Results indicated that the currents was maintained 98.1, 97.8, 95.3, 93.2 and 90.8% of the initial signal after storage of 20, 40, 60, 80 and 100 days with satisfactory stability.

Monitoring of target NGAL in human serum samples and urine

To elucidate the method accuracy relative to commercial human lipocalin-2/NGAL ELISA kit, PB-g-C_3N_4-based electrochemical immunoassay was used for analysis of target NGAL in human serum samples and urine (note: Human serum specimens and urine were obtained from our hospital according to the rules of the local ethical committee; Informed consent was obtained from all individual participants including in this study). Typically, NGAL is secreted into the urine by the thick ascending limb of loop of Henle and collecting ducts of kidney, with synthesis occurring in the distal nephron [29]. Owing its small molecular size, NGAL is freely filtered and can be easily detected in urine. Thereafter, the results from our strategy were compared with those from commercial human lipocalin-2/NGAL ELISA kit by the application of an *F*-test and the linear regression equation between the average values per sample. As shown from Table 2, the t_{exp} values in all cases were below t_{crit} ($t_{crit[4, 0.05]} = 2.77$), and the regression equation was fitted to $y = 0.8982\times + 0.1512$ ($R^2 = 0.9977$, $n = 8$) (note: *x*-axis for the electrochemical immunoassay and *y*-axis for human lipocalin-2/NGAL ELISA kit). The slope and intercept of the regression equation were close to the ideal '1' and '0', respectively. Thus, the method accuracy of our system was acceptable for the detection of complex biological fluids.

Conclusions

In summary, this work demonstrated the development of an electrochemical immunoassay by using Prussian blue-decorated g-C_3N_4 nanohybrids for signal amplification. Introduction of Prussian blue nanoparticles as the signal-generation tags efficiently avoided the participation of natural natures. The g-C_3N_4 with high surface coverage provides a large room for conjugation of the indicator and biomolecule.

Table 2 Evaluation of method accuracy with commercial human lipocalin-2/NGAL ELISA kit for human serum specimens and urine

Type	No.	Method; Conc. [mean ± SD (RSD), ng·mL^{-1}, $n = 3$][a]		t_{exp}
		Immunosensor	ELISA kit	
Human serum	1	3.2 ± 0.11 (3.44%)	3.3 ± 0.09 (2.73%)	1.22
	2	0.12 ± 0.02 (16.67%)	0.16 ± 0.02 (12.5%)	2.45
	3	4.5 ± 0.3 (6.67%)	4.2 ± 0.2 (4.76%)	1.44
	4	12.3 ± 1.1 (8.94%)	11.1 ± 1.1 (9.91%)	1.34
Human urine	1	0.34 ± 0.02 (5.88%)	0.29 ± 0.03 (10.34%)	2.41
	2	1.2 ± 0.2 (16.67)	1.4 ± 0.1 (7.14%)	1.55
	3	5.6 ± 0.6 (10.71%)	5.3 ± 0.5 (9.43%)	0.67
	4	2.4 ± 0.3 (12.5%)	2.1 ± 0.2 (9.23%)	1.44

[a] Analyses were made in triplicate according to the diluted ratio, and the data were obtained as mean values of three assays ($n = 3$)

Relative to graphene nanosheets, the existed N element in g-C_3N_4 nanosheets enhanced electrocatalytic efficiency of the nanohybrids thanks to the lone-pair electrons [30, 31]. Although the present work focused on detection of target NGAL, it easily extends to determine other cancer biomarkers by controlling the corresponding antibodies. Nevertheless, one limitation of this work is the relatively long assay time per sample. Therefore, future work should focus on the improvement of the detection steps.

Funding information Support by the Health Science Research Personnel Training Program of Fujian Province (Grant no.: 2017-CXB-22) and the Scientific Research Innovation Team Construction Program of Fujian Normal University (Grant no.: IRTL1702) is gratefully acknowledged.

Compliance with ethical standards The authors declare that they have no competing interest.

References

1. Pisano D, Joyce M (2018) Plasma neutrophil gelatinase-associated lipocalin: biomarker of the future or just another test? J Clin Anesthesia 45:37–38
2. Hraba-Renevey S, Turler H, Kress M, Salomon C, Weil R (1989) SV40-induced expression of mouse gene 243 involves a post-transcriptional mechanism. Oncogene 4:601–608
3. Mori K, Nakao K (2007) Neutrophil gelatinase-associated lipocalin as the real-time indicator of active kidney damage. Kidney Int 71: 967–970
4. Deverajan P (2010) Neutrophil gelatinase-associated lipocalin: a promising biomarker for human acute kidney injury. Biomark Med 4(2):265–280
5. Sellmer A, Bech B, Bjerre J, Schmidt M, Hjortdal V, Esberg G, Rttig S, Henriksen T (2017) Urinary neutrophil gelatinase-associated lipocalin in the evaluation of patent ductus arteriosus and AKI in very preterm neonates: a cohort study. BMC Pediatr 17:art. ID 7
6. Devarajan P (2008) Neutrophil genlatinase-associated lipocalin (NGAL): a new maker of kidney disease. Scand J Clin Lab Invest Suppl 241:89–94
7. Lei L, Zhu J, Xia G, Feng F, Zhang H, Han Y (2017) A rapid and user-friendly assay to detect the neutrophil gelatinase-associated lipocalin (NGAL) using up-converting nanoparticles. Talanta 162: 339–344
8. Shukla K, Badgujar S, Bhanushali P, Sabharwal S (2017) Simplified purification approach of urinary neutrophil gelatinase-association lipocalin by tangential flow filtration and ion exchange chromatography. J Chromatogr B 1051:68–74
9. Mu Y, Xie H, Wan Y (2015) Sensitive and specific neutrophil gelatinase-associated lipocalin detection by solid-phase proximity ligation assay. Anal Sci 31:475–479
10. Li H, Mu Y, Yan J, Cui D, Ou W, Wan Y, Liu S (2015) Label-free photoelectrochemical immunosensor for neutrophil gelatinase-associated lipocalin based on the use of nanobodies. Anal Chem 87:2007–2015
11. Kannan P, Tiong H, Kim D (2012) Highly sensitive electrochemical detection of neutrophil gelatinase-associated lipocalin for acute kidney injury. Biosens Bioelectron 31:32–36
12. Qiu Z, Shu J, Tang D (2018) Near-infrared-to-ultraviolet light-mediated photoelectrochemical aptasensing platform for cancer biomarker based on core-shell $NaYF_4$:Yb,tm@TiO_2 upconversion microrods. Anal Chem 90:1021–1028
13. Shu J, Tang D (2017) Current advances in quantum-dots-based photoelectrochemical immunoassay. Chem Asian J 12:2780–2789
14. Zhang K, Lv S, Lin Z, Li M, Tang D (2018) Bio-bar-code-based photoelectrochemical immunoassay for sensitive detection of prostate-specific antigen using rolling circle amplification and enzymatic biocatalytic precipitation. Biosens Bioelectron 101:159–166
15. Gao Z, Lv S, Xu M, Tang D (2017) High-index: HK_0 faceted platinum concave nanocubes with enhanced peroxidase-like activity for an ultrasensitive colorimetric immunoassay of the human prostate-specific antigen. Analyst 142:911–917
16. He L, Guo C, Song Y, Zhang S, Yang M, Peng D, Fang S, Zhang Z, Liu C (2017) Chitosan stabilized gold nanoparticle based electrochemical ractopamine immunoassay. Microchim Acta 184:2919–2924
17. Shu J, Qiu Z, Lv S, Zhang K, Tang D (2018) Plasmonic enhancement coupling with defect-engineered TiO_{2-x}: a mode for sensitive photoelectrochemical biosensing. Anal Chem 90:2425–2429
18. Qin Z, Xu W, Chen S, Chen J, Qiu J, Li C (2018) Electrochemical immunoassay for the carcinoembryonic antigen based on the use of a glassy carbon electrode modified with an octahedral Cu_2O-gold nanocomposite and staphylococcal protein for signal amplification. Microchim Acta 185:266
19. Yin S, Zhao L, Ma Z (2018) Label-free electrochemical immunosensor for ultrasensitive detection of neuron-specific enolase based on enzyme-free catalytic amplification. Anal Bioanal Chem 410:1279–1286
20. Felix F, Angnes L (2018) Electrochemical immunosensors-a powerful tool for analytical applications. Biosens Bioelectron 102:470–478
21. Chu Z, Liu Y, Jin W (2017) Recent progress in Prussian blue films: methods used to control regular nanostructures for electrochemical biosensing applications. Biosens Bioelectron 96:17–25
22. Wen S, Wang Y, Yuan Y, Liang R, Qiu J (2018) Electrochemical sensor for arsenite detection using graphene oxide assisted generation of Prussian blue nanoparticles as enhanced signal label. Anal Chim Acta 1002:82–89
23. Aguila D, Prado Y, Koumousi E, Mathoniere C, Clerac R (2016) Switchable Fe/co Prussian blue networks and molecular analogues. Chem Soc Rev 45:203–224
24. Moritomo Y, Takachi M, Kuihara Y, Matsuda T (2013) Synchrotron-radiation X-ray investigation of li^+/Na^+ intercalation into Prussian blue analogues. Adv mater Sci Engin 2013: art. ID 967285
25. Mollarasouli F, Serafin V, Campuzano S, Yanez-Sedeno P, Pingarron J, Asadpour-Zeynali K (2018) Ultrasensitive determination of receptor tyrosine kinase with a label-free electrochemical immunosensor using graphene quantum dots-modified screen-printed electrodes. Anal Chim Acta 1011:28–34
26. Molinero-Abad B, Izquierdo D, Perez L, Escudero I, Arcos-Martinez M (2018) Comparison of backing materials of screen printed electrochemical sensors for direct determination of the subnanomolar concentration of lead in seawater. Talanta 182: 549–557
27. Lv S, Li Y, Zhang K, Lin Z, Tang D (2017) Carbon dots/g-C_3N_4 nanoheterostructures-based signal-generation tags for photoelectrochemical immunoassay of cancer biomarkers coupling with copper nanoclusters. ACS Appl Mater Interface 9:38336–38343
28. Ouyang H, Tu X, Fu Z, Wang W, Fu S, Zhu C, Du D, Lin Y (2018) Colorimetric and chemiluminescent dual-readout immunochromatographic assay for detection of pesticide

utilizing g-C_3N_4/$BiFeO_3$ nanocomposites. Biosens Bioelectron 106:43–49
29. Wasilewaka A, Zoch-Zwierz W, Taranta-Janusz K, Michaluk-Skutnik J (2010) Neutrophil gelatinase-associated lipocalin (NGAL): a new marker of cyclosporine nephrotoxicity? Pediatr Nephrol 25:889–897
30. Zheng Y, Jiao Y, Jaroniec M, Jin Y, Qiao S (2012) Nanostrucrued metal-free electrochemical catalysts for highly efficient oxygen reduction. Small 8:3550–3566
31. Gong Y, Li M, Wang Y (2015) Carbon nitride in energy conversion and storage: recent advances and future prospects. ChemSusChem 8:931–946